11th International Conference on Fracture Mechanics of Concrete and Concrete Structures
FraMCoS-11
J. M. Chandra Kishen, A. Ramaswamy, S. Ray and R. Vidyasagar (Eds)
https://doi.org/10.21012/FC11.092349

ACOUSTIC EMISSION ATTENUATION IN SINGLE-MIX AND FUNCTIONALLY LAYERED CONCRETE SLABS

SAM H. COCKING[*], MAR GIMÉNEZ FERNÁNDEZ[*], NIKOLAOS I. TZIAVOS[†], AND JANET M. LEES[*]

[*] Department of Engineering, University of Cambridge
Civil Engineering Building, JJ Thomson Avenue 7a, Cambridge, CB3 0FA, UK
e-mail: sc740@cam.ac.uk, www.cirg.eng.cam.ac.uk

[†] Department of Civil Engineering, School of Infrastructure and Sustainable Engineering
Aston University, Birmingham, B4 7ET, UK
e-mail: n.tziavos@aston.ac.uk, www.aston.ac.uk

Key words: Acoustic Emissions, Non-Destructive Testing, Functionally Graded Concrete

Abstract: The carbon intensity of cement production motivates new techniques for concrete construction. These include functional layering, in which multiple concrete mixes are used to cast a single element. For functional layering to be adopted in practice, it is first necessary to understand how material behaviour and damage mechanisms are affected by this construction approach. In this paper, Acoustic Emission (AE) signals from pencil lead break tests are studied for a set of single-mix and layered concrete slabs. For the single-mix slabs, the findings demonstrate the influence of mix design on AE parameters and attenuation in concrete. Parameter variation in a horizontally layered slab is then predicted, using fitted models of behaviour from the single-mix slabs. These predictions agree best with measurement data in regions where most of the material under consideration is the higher-attenuating mix. When this is not the case, agreement is poorer, suggesting that the presence of the interlayer boundaries may give rise to other wave phenomena which influence AE attenuation.

1 INTRODUCTION

Concrete is a major construction material – the most heavily used in the world – and production of the cement needed to make concrete accounts for approximately 5% of global CO_2 emissions. One of the most promising avenues for reducing this cement use is Functionally Graded, or Layered, Concrete (FGC) [1]. More than one concrete mix is used in the manufacture of FGC elements, with the spatial distribution of these mixes targeted to achieve the desired properties. For example, higher cement concretes may be beneficial around the exterior of an element to create a 'durability layer' which protects against carbonation or chloride ingress, while a lower cement – and, therefore, lower carbon – mix may well be adequate for the interior region [2].

The distribution of multiple concrete mixes throughout a single element has consequences for the potential mechanisms of damage which this element may go on to experience [3]. It is therefore imperative to develop our understanding of damage and deterioration in FGC, including how this may deviate from the behaviour of single-mix concretes, if industry is to confidently adopt FGC in practice. Structural Health Monitoring (SHM) and Non-Destructive Testing (NDT) are key approaches that can be used to develop this understanding.

For years, Acoustic Emission (AE) testing has been known to be a promising SHM

technique for damage detection in concrete structures (see e.g., [4] and [5]). This technique measures the energy that is released in a solid when damage, such as cracking, causes the creation of new surface area. Specifically, following such damage, elastic waves propagate through the material to its surface, where they can be detected using piezoelectric sensors. Often, pencil lead break (PLB) tests are initially used to induce these elastic waves, allowing the attenuation of AE signals at various propagation distances from a sensor to be studied. Applications of AE sensing include damage localisation and source identification, damage severity evaluation, and failure prediction [6].

However, for this method to be properly applied to FGC structures, it is critical to understand how their variation in material behaviour may influence AE signals, compared to single-mix concretes. For instance, the constituent concretes in an FGC element may attenuate AE waves differently, while the influence of interlayer boundary regions between two adjacent concrete mixes is not yet known.

In this paper, the attenuation of AE waves has been studied for a set of single-mix and layered slabs. Specifically, AE sensors were used to measure the waveforms of burst signals induced by PLB tests over various propagation distances, as part of a broader test series conducted on these slabs [7]. Here, relationships for attenuation and AE parameter variation are derived and interpreted.

Although AE attenuation has previously been reported for single-mix unreinforced [8] and reinforced [9] concretes, this is the first time that Acoustic Emissions have been studied in FGC structures.

2 METHODOLOGY

2.1 Experimental specimens

In [7], a set of single-mix and functionally layered concrete slabs were tested to failure in four-point bending, to quantify the effects of functional layering on structural performance and evaluate a proposed design methodology for FGC slab construction. That study presented and interpreted results from a wide range of instrumentation, including strain gauges, fibre-optic strain monitoring, and LED large field dynamic measuring machine (DMM) displacement monitoring. AE monitoring was also conducted during this test series. However, detailed analysis and interpretation of the AE data was beyond the scope of [7].

Figure 1 shows the subset of slabs from [7] which are considered in this paper. Slabs (a) and (b) are conventional, single-mix slabs, constructed using low-cement and high-cement concretes respectively. These two mixes are then layered horizontally in (c), with the low-cement mix cast wet-on-wet above the high-cement mix.

Multiple copies of the single-mix slabs were cast and tested. In this paper, data are studied from two low-cement slabs and three high-cement slabs. Only one copy of the FGC slab was manufactured.

Note that Figure 1 shows the transverse cross-sections of these slabs, which each had a length of 1200 mm and were ultimately tested in flexure about this longitudinal axis. As shown in Figure 1, each slab also contained longitudinal reinforcement, in the form of four steel bars of 8 mm diameter.

Table 1 shows the mix designs of the low- and high-cement concretes used in these slabs. These concretes show clear differences in their water/binder ratios: 0.8 and 0.4 respectively, for the low- and high-cement mixes. They also use different ratios of total aggregate/binder: 9.1 for the low-cement mix, compared to 2.4 for the high-cement mix. Note that the ratios of coarse/fine aggregate are very similar for both mixes, at approximately 0.5.

For each slab, material properties were reported in [7]. On average, the low-cement mix displayed an elastic modulus of 23.6 GPa and compressive cube strength of 18.0 MPa. The corresponding values for the high-cement mix were 35.2 GPa and 66.1 MPa.

2.2 Acoustic Emission sensing

AE testing of these slabs was performed

using a Mistras Express8 Micro-II monitoring system and eight R6I sensors. This included PLB tests to study AE attenuation in the slabs, which were conducted prior to the structural (four-point bending) tests. PLBs were performed at distances of 50, 100, and 150 mm from each of the eight AE sensors, when this was possible given the slab geometry.

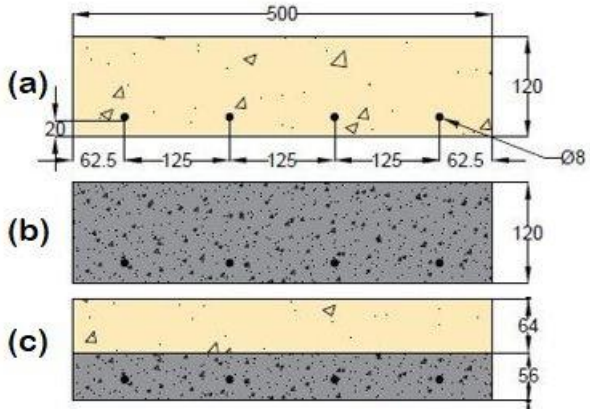

Figure 1: Slabs designs (a) to (c) that have been considered in this study, with dimensions in mm (adapted from [7]).

Table 1: Concrete mix designs used in these slab experiments

Mix name:	Mix proportions (kg/m^3)			
	Cement	Fine aggregate	Coarse aggregate	Water
Low cement	225	1346	694	180
High cement	625	994	476	250

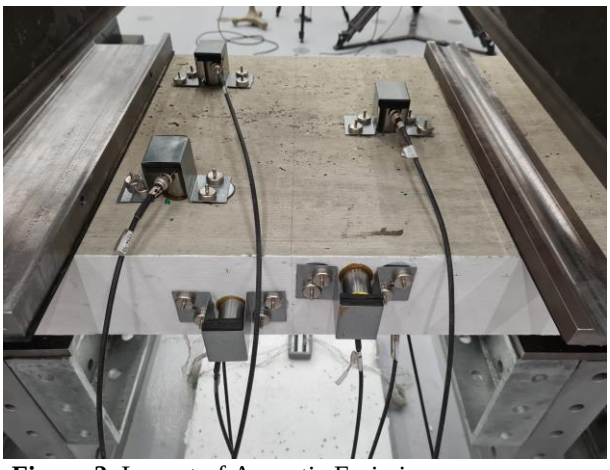

Figure 2: Layout of Acoustic Emission sensors on one of the concrete slabs (from [7])

Figure 2 shows one of the concrete slabs before a test, with these AE sensors in situ. Each sensor contains an integral 40 dB pre-amplifier with an operational frequency range of 40-100 kHz. These low-noise sensors are reported to have a maximum referred-to-input root mean square (RMS) noise level of 3 µV.

Due to the volume of acquired AE data during a destructive test, AE waveform processing becomes a challenging task. For this reason, parameter-based AE analysis was developed as an alternative to waveform-based analysis. Using this approach, a parametric summary is calculated and saved for each AE hit, instead of the entire waveform. While modern sensors and data loggers make waveform-based AE sensing possible, the parametric method remains popular.

In this paper, the following AE parameters have been studied:

- **Amplitude [dB]**: the peak amplitude of the AE signal.
- **Average signal level (ASL) [dB]**: the RMS signal voltage for a measured event.
- **Rise time [µs]**: the time between the AE signal first passing the measurement threshold and reaching its peak amplitude.
- **Counts**: the number of times the AE signal exceeds the measurement threshold during a single hit.
- **Signal strength [pVs]**: the time integral of the absolute voltage signal, before any amplification.
- **Absolute energy [aJ]**: the time integral of the square of the voltage signal, divided by a 10 kΩ impedance and before any amplification.

These parameters are expected to vary spatially with propagation distance x, which is the distance between the sensor and the location of an AE source, such as a cracking event or a PLB. In this study, exponential variation has been investigated, in keeping with previous studies on AE parameter variation in concretes [8]. This takes the general form given in Equation 1, in which a and b are constants to be found during the PLBs.

$$y = a\, e^{bx} \quad (1)$$

In the following sections, PLB data are plotted and used to fit exponential relationships that describe the six AE parameters above. Parameter variation in the low- and high-cement single-mix slabs ((a) and (b) in Figure 1) is then interpreted, based on the composition and material properties of each slab. Finally, these models for each concrete mix are used to predict the behaviour in a functionally layered slab cast using both mixes.

2.3 Fitting the paramter relationships

Three fitting algorithms were trialled during this study, which treated outliers as follows:

1. **Unweighted linear least-squares**: data points are given no weighting and the model parameters are found using a standard, linear least-squares fitting procedure.
2. **Weighted bisquare least-squares**: weights are assigned based on the distance of data points from the fitted model, with reduced weight corresponding to increased distance. Beyond the distance that could be explained by random chance, points have zero weight. The fitting procedure seeks to minimise the weighted sum of the squares of the residuals.
3. **Least absolute residuals (LAR)**: the fitted model is found by minimising the (unweighted) absolute residuals of the data points, instead of their squares. As a result, outliers have less influence on the fitting procedure.

It was found that LAR consistently gave models with the highest goodness of fit, as expressed by their R^2 values. Only these models are reported in this paper.

3 RESULTS AND DISCUSSION

3.1 AE parameters in the low-cement slab

Figure 3 plots the fitted parameter relationships for the low-cement slab, alongside the measurement data from the PLBs that have been used to obtain these models. Mean and median values of the experimental data are plotted in red and blue dashed lines, respectively.

The influence of high-magnitude outliers on the means can be seen for all parameters except for the amplitude (see Figure 3(e)), especially at a propagation distance of 50 mm. Note that some outliers lie beyond the axis limits of these plots, while other data are clustered together at similar magnitudes; these attributes can be seen more clearly in the data distributions considered in Figure 6 (see Section 3.4). In contrast to the means, the median values of the experimental data tend to lie close to the fitted exponential models, which are plotted in black solid lines.

Figure 3 includes R^2 values of the fitted models, which display very high goodness of fit for all parameters other than the amplitude. Potential reasons for this are discussed in section 3.4. It was found that the fitting methods discussed in section 2.3 all led to very similar models for the attenuation of the signal amplitude, which was not the case for the other AE parameters considered in this study.

3.2 AE parameters in the high-cement slab

Figure 4 reproduces the plots of Figure 3 using the data and fitted models for the high-cement slab. The comments made in section 3.1, regarding goodness of fit and the influence of outliers on the mean values, also apply to the high-cement slab in Figure 4.

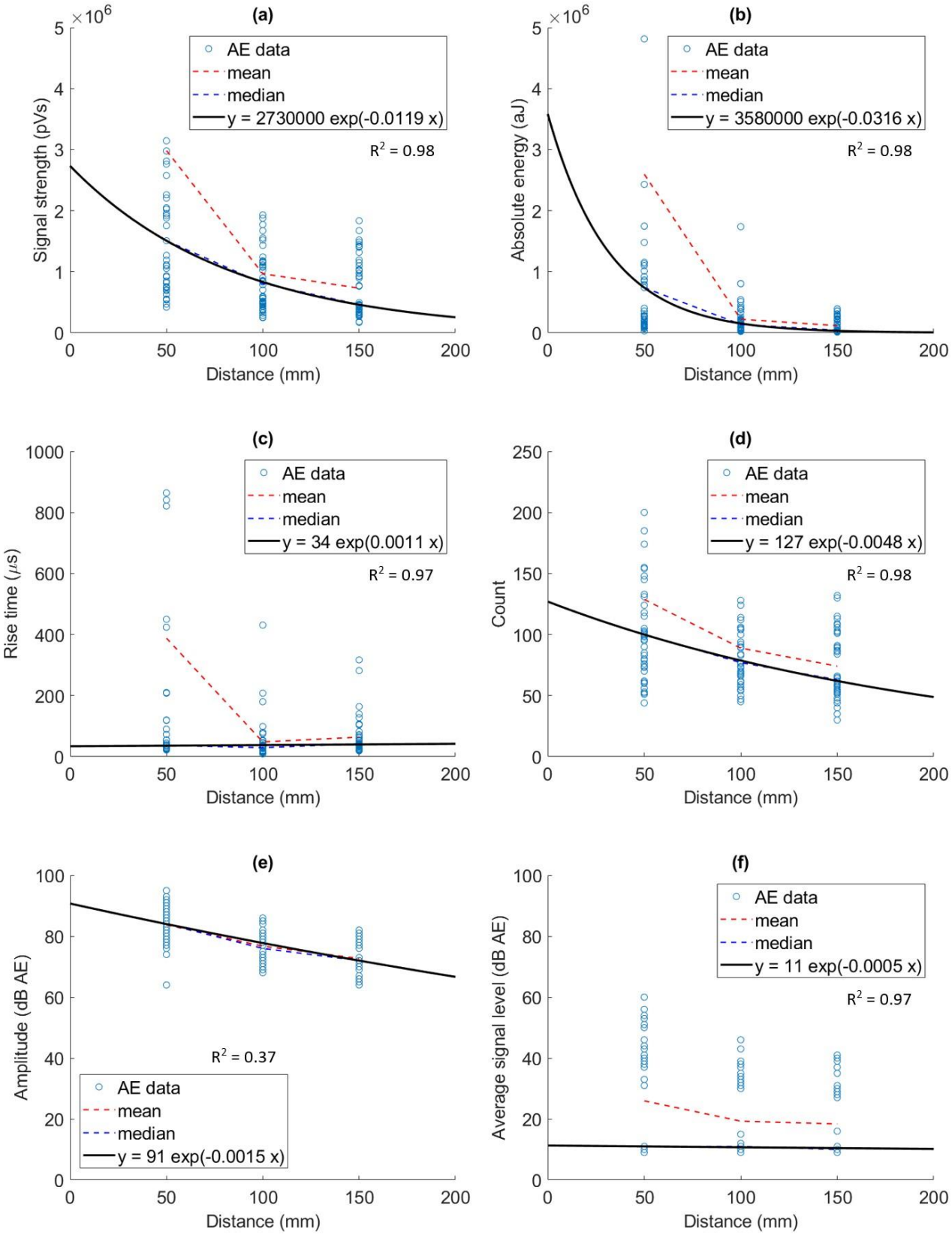

Figure 3. AE parameter variation relationships for the single-mix, low-cement slab, for (a) signal strength, (b) absolute energy, (c) rise time, (d) count, (e) amplitude, and (f) average signal level (ASL)

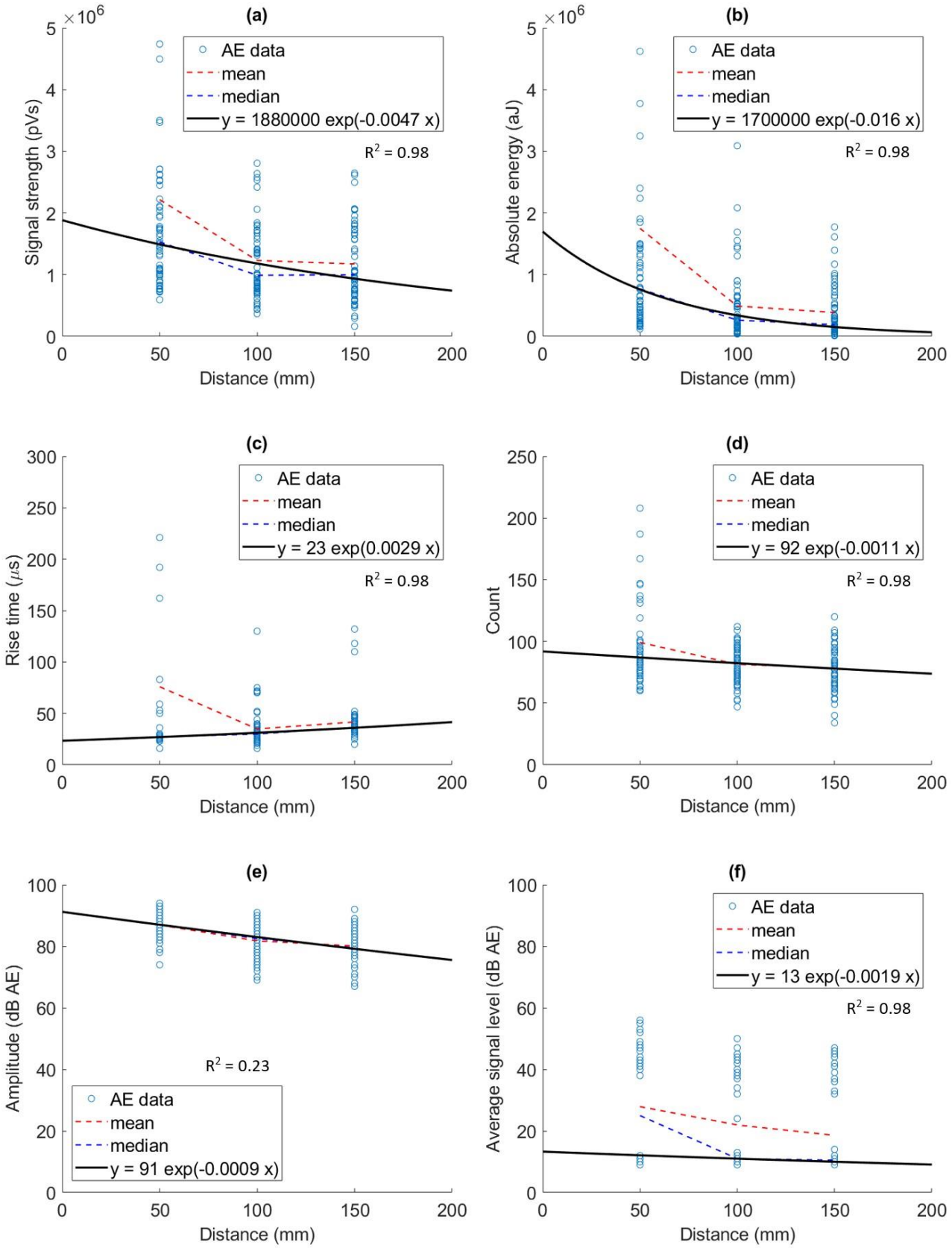

Figure 4. AE parameter variation relationships for the single-mix, high-cement slab, for (a) signal strength, (b) absolute energy, (c) rise time, (d) count, (e) amplitude, and (f) average signal level (ASL)

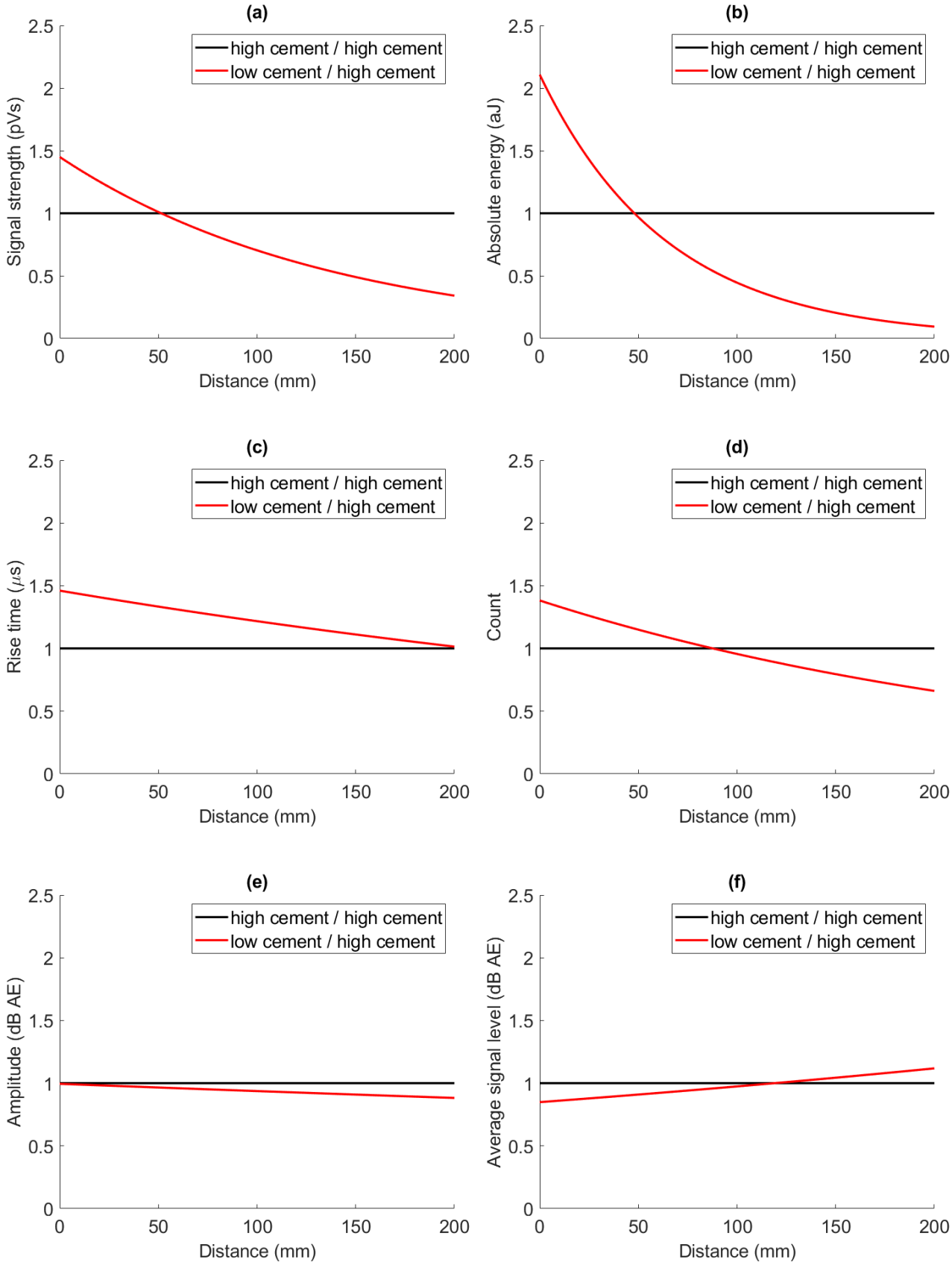

Figure 5. Comparison of AE parameter variation in the single-mix low- and high-cement slabs, obtained by normalising the fitted relationships with respect to those of the high-cement slab; results are shown for (a) signal strength, (b) absolute energy, (c) rise time, (d) count, (e) amplitude, and (f) average signal level (ASL)

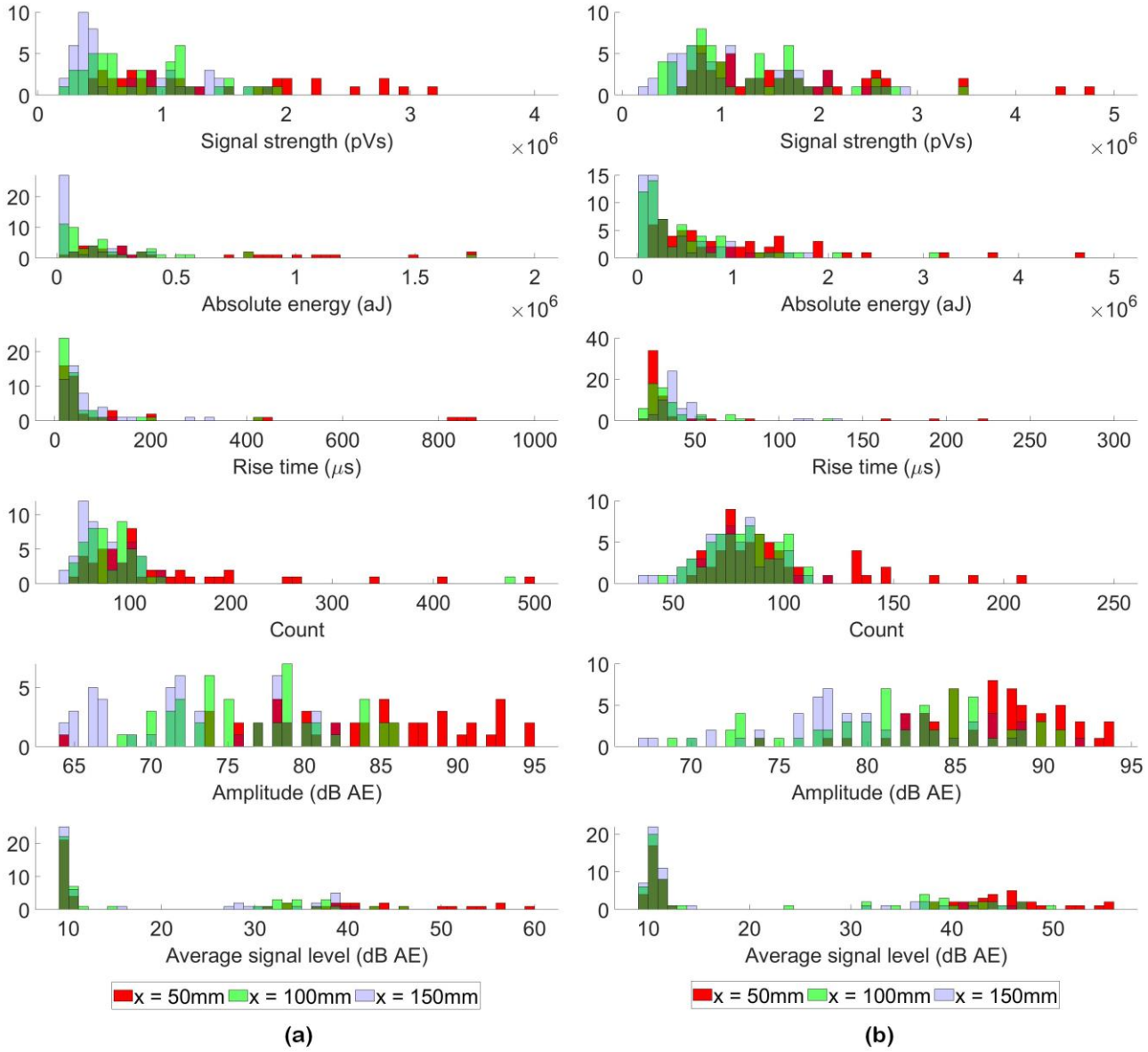

Figure 6. Distributions of the AE parameter measurements, for the single-mix (a) low-cement and (b) high-cement slabs

3.3 Influence of concrete mix design on AE parameters

Figure 5 contrasts AE parameter variation in the low- and high-cement concrete slabs by plotting the fitted models for both concretes, after these have been normalised with respect to the high-cement slab.

At low propagation distances, it is observed that the magnitudes of the signal strength, absolute energy, rise time, and count are all higher for the low-cement slab. In contrast, the ASL of the high-cement slab is initially slightly higher, while the peak signal amplitudes are very similar for both mixes.

As well as often displaying higher initial magnitudes, Figure 5 shows that all parameters except for the ASL show greater decay over shorter distances in the low-cement slab. This can be interpreted in terms of the mix designs of the two concretes. As stated in section 2.1, the water/binder ratio of the low-cement concrete mix is double that of the high-cement mix, while its aggregate/binder ratio is almost four times higher.

Both differences could lead to higher attenuation of AE signals in the low-cement slab. Firstly, the higher relative amount of

water in the low-cement concrete is likely to lead to higher porosity in its hardened state, as it is more probable that there will be excess water which will ultimately evaporate and leave behind voids. These voids will impede the transmission of AE waves within the concrete. Secondly, it was identified in [8] that larger aggregate particle sizes lead to greater AE attenuation in concretes. While the ratios of coarse/fine aggregate are similar for both mixes in this study, the much higher ratio of total aggregate/binder in the low-cement concrete means that it will contain a higher absolute quantity of coarse aggregate. Therefore, this effect will also lead to higher amplitude decay over smaller distances in the low-cement slab, relative to the high-cement slab.

These stark differences highlight the influence of concrete mix design on AE attenuation and parameter variation, with important consequences for the interpretation of AE sensing data.

3.4 Statistical variation of the measured AE parameters

As mentioned earlier (see section 3.1), the measured peak amplitudes of the AE signals in both single-mix slabs were considerably harder to fit with exponential attenuation models. Different fitting algorithms produced very similar model predictions, with consistently low R^2 values. In contrast, changing the fitting procedure led to significantly different models for all other AE parameters. As discussed in section 2.3, the key difference between these procedures is their approach to data with extreme values (i.e., outliers).

To investigate the statistical distributions of the measured AE parameters, Figure 6 plots histograms of these data for the two slabs. Each subplot shows the distribution of an AE parameter, with data corresponding to propagation distances of 50, 100, and 150 mm plotted in red, green, and blue respectively. The distributions of all parameters except for the amplitude have a heavy right tail; that is, they contain high-magnitude outliers. It is reasonable that these parameters would be best captured by models that use a robust fitting method, such as LAR.

In contrast, the amplitude data show reasonably symmetric distributions in Figure 6, and there are few clear outliers. It has already been seen in Figures 3 and 4 that the mean and median values of the amplitude agree well, for both slabs, which suggests few extreme values in these measurements. Statistical spread remains in these data, however, as evidenced by the low R^2 values of the fitted models. This may be due to variability of the concrete material throughout, and between, the slabs that have been tested.

3.5 AE parameters in the FGC slabs

The fitted models of AE parameter variation in the two single-mix concrete slabs can now be used to predict behaviour in the functionally layered slab cast using both mixes. In Figure 7, experimental data and model predictions are compared for slab (c), in which the low-cement mix has been horizontally layered above the high-cement mix (c.f. Figure 1). This slab was cast wet-on-wet, allowing for the development of better bond between the two layers.

Figure 7 presents data from two AE sensors. Sensor 1 is located on the low-cement layer, 21 mm from the interlayer boundary, and records the response to PLBs performed on the high-cement layer. Sensor 2 is located 6 mm from the interlayer boundary, on the high-cement layer, and measures PLBs initiated in the low-cement layer. For both sensors, the propagation distance for the PLBs was 50 mm.

In Figure 7, data points from PLBs are plotted as circles while solid lines show the modelled predictions of parameter variation. These are based on variation occurring at different rates in the two layers, in line with the behaviour of the corresponding single-mix slabs. Data and models for sensor 1 are plotted in blue, while for sensor 2 these are plotted in red. Dotted black lines show the two single-mix models that have been used to generate these FGC predictions.

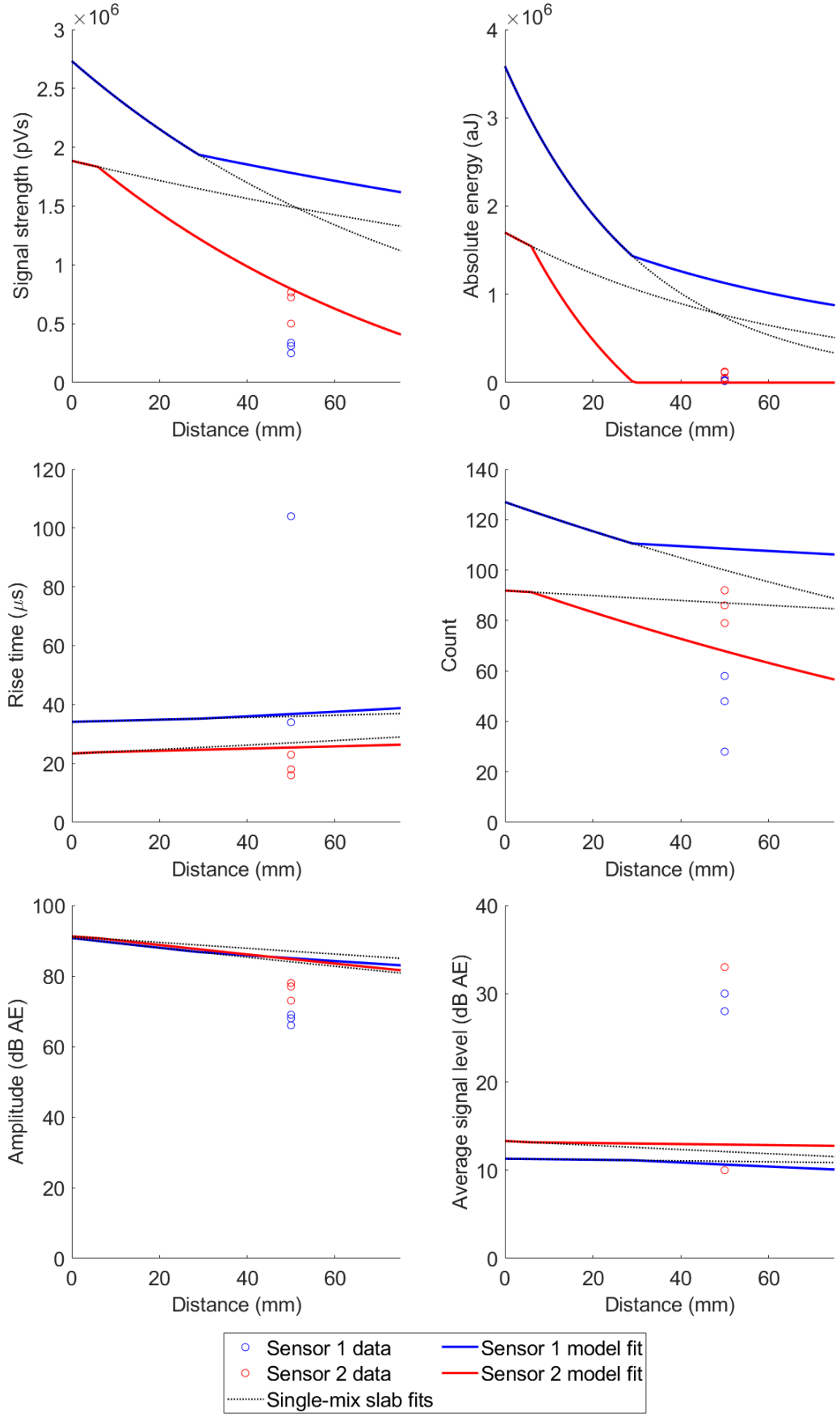

Figure 7. Measurement of AE parameter variation across the interlayer boundary in FGC slab (c), with sensors detecting PLBs conducted in (1) the high-cement mix and (2) the low-cement mix

Considering the signal strength and absolute energy, the data show greater magnitude decay than can be explained by either single-mix model on its own. Data from the two sensors are similar in magnitude; for sensor 2, these are in line with the FGC predictions, while there is notable disagreement for sensor 1. Possible explanations could be that the higher parameter decay in the low-cement mix is dominating the behaviour, despite the presence of functional layering, or that there are additional attenuating effects in the FGC slab due to the presence of the interlayer boundary. Studying the potential for such effects is beyond the scope of this paper but warrants further research.

Note that region of the slab considered in the PLBs for sensor 2 is skewed towards the low-cement mix, while the corresponding region for sensor 1 is more evenly balanced between the two mixes. Based on this, and from examination of Figure 5, it is reasonable to expect that signal strength and absolute energy would be lower for sensor 1, as Figure 7 shows.

Examining the other AE parameters for sensor 1, relative to sensor 2, Figure 7 shows that sensor 1 also records fewer counts and slightly lower signal amplitude, which can both be related to the lower energy and signal strength observed by this sensor. For the counts, this may be anticipated based on the trends in Figure 5, while the two sensors would be expected to record similar amplitudes.

Figure 5 would also lead to a prediction of lower rise time and higher ASL for sensor 1; however, these are not seen in Figure 7. For ASL, this difference is not expected to be significant and comparison with data is made more challenging by the spread in the measurements. For rise time, this may be another indication of further phenomena affecting the transmission of AE waves at the interlayer boundary. Again, this warrants further research.

4 CONCLUSIONS

This study has investigated the attenuation of AE waves, and spatial variation of AE parameters, in a series of concrete slabs through analysis of PLB data. Initially, two single-mix slabs were examined, which were cast using low- and high-cement concretes respectively. Exponential relationships were fitted to the data, to describe the variation of AE parameters in these slabs. High goodness of fit was achieved for all parameters except for the peak signal amplitude; in this particular case, symmetric spread in the data meant that models could not be fitted which adequately explained most of the measurements.

Most AE parameters exhibited higher initial magnitudes and greater spatial variation in the low-cement slab, which can be explained by considering the mix design of this concrete. It is reasonable to expect greater attenuation in the low-cement concrete, on the basis of its higher water/binder and aggregate/binder ratios.

In the layered slab, signal strength and absolute energy were observed to decay to a greater extent than could be explained by either of the single-mix models of parameter variation. The effect of layering on the spatial variation of the signal counts can also be seen, while its effect on the other parameters – rise time, amplitude, and ASL – is harder to discern, in part because there is less anticipated variation of these parameters between the two mixes.

As discussed in section 3.5, the modelled FGC predictions in this study have been based purely on parameter variation occurring at different rates in the two mixes. There may be further effects, introduced in the interlayer boundary region due to the layered construction, which also affect transmission of AE waves. Such effects go beyond the scope of this paper and will be studied in future research.

ACKNOWLEDGEMENTS

This project was supported by funding from the UK Engineering and Physical Sciences Research Council (EPSRC). This includes

PhD funding from the University of Cambridge EPSRC-funded *Centre for Doctoral Training in Future Infrastructure and Built Environment* (grant number EP/L016095/1), and EPSRC Research Award EP/N017668/1: *Tailored Reinforced Concrete Infrastructure: Boosting the Innate Response to Chemical and Mechanical Threats*.

REFERENCES

[1] G. Torelli, M. Giménez Fernández, and J.M. Lees, 2020. Functionally graded concrete: Design objectives, production techniques and analysis methods for layered and continuously graded elements, *Construction and Building Materials*, 242, 118040.

[2] J. Forsdyke and J.M. Lees, 2022. An analysis of the potential for improving cement efficiency through functionally graded concrete elements with durability-driven concrete specification, in: *IABSE Symposium Prague*.

[3] M.W.T. Mak and J.M. Lees, 2023. Carbon reduction and strength enhancement in functionally graded reinforced concrete beams, *Engineering Structures*, 277, 115358.

[4] C. Grosse, H. Reinhardt, and T. Dahm, 1997. Localization and classification of fracture types in concrete with quantitative acoustic emission measurement techniques, *NDT&E International*, 30, 223-230.

[5] S. Colombo, I.G. Main, and M.C. Forde, 2003. Assessing Damage of Reinforced Concrete Beam Using "b-value" Analysis of Acoustic Emission Signals, *Journal of Materials in Civil Engineering*, 15, 280-286.

[6] A. Behnia, H.K. Chai, and T. Shiotani, 2014. Advanced structural health monitoring of concrete structures with the aid of acoustic emission, *Construction and Building Materials*, 65, 282–302.

[7] M. Giménez Fernández, 2022. Design and Performance of Reinforced Concrete Elements with Spatial Tailoring of Concrete Properties, PhD thesis, University of Cambridge.

[8] X. Wu, Q. Yan, A. Hedayat, and X Wang, 2021. The influence law of concrete aggregate particle size on acoustic emission wave attenuation, *Sci Rep*, 11, 22685.

[9] H. Feng and W. Yi, 2017. Propagation characteristics of acoustic emission wave in reinforced concrete, *Results in Physics*, 7, 3815-3819.